Analysis of the behavior of 2D monolayers and 3D spheroid human pancreatic beta cells derived from induced pluripotent stem cells in a microfluidic environment

Amal Essaouiba, Rachid Jellali, Marie Shinohara, Benedikt Scheidecker, Cécile Legallais, Yasuyuki Sakai, Eric Leclerc

Analysis of the behavior of 2D monolayers and 3D spheroid human pancreatic beta cells derived from induced pluripotent stem cells in a microfluidic environment

Amal Essaouiba[1,2], Rachid Jellali[1], Marie Shinohara[3], Benedikt Scheidecker[3], Cécile Legallais[1], Yasuyuki Sakai [2,3], Eric Leclerc[1,2(*)]

[1]*Université de technologie de Compiègne, CNRS, Biomechanics and Bioengineering, Centre de recherche Royallieu CS 60319, 60203 Compiègne Cedex*

[2]CNRS UMI 2820; Laboratory for Integrated Micro Mechatronic Systems, Institute of Industrial Science, University of Tokyo; 4-6-1 Komaba; Meguro-ku; Tokyo, 153-8505, Japan

[3]Department of Chemical Engineering, Faculty of Engineering, University of Tokyo, 7-3-1 Hongo, Bunkyo-ku, Tokyo 113-8656, Japan

*** Corresponding author**

Eric Leclerc: eleclerc@iis.u-tokyo.ac.jp, eric.leclerc@utc.fr

Rachid Jellali: rachid.jellali@utc.fr

Abstract

The limited availability of primary human β-cells/islets and their quality (due to donor diversity) restrict the development of *in vitro* models for diabetes research. Human induced pluripotent stem cells (hiPSCs) may be a promising cell-source for diabetes studies, anti-diabetic drug screening and personalized therapies. However, achieving levels of maturity/functionality that are comparable to the *in vivo* situation and islets rebuilt from iPSCs is still challenging. Here, we compare and discuss two strategies for culturing human pancreatic β-cells derived from hiPSCs in microfluidic biochips. First, we confirmed that the protocol in conventional Petri 2D monolayer led to insulin, PDX1 and MAFA positive staining, to C-Peptide productive cells, and to tissue responsive to high/low glucose and GLP1 stimulation. This protocol and its subsequent modifications (including extracellular matrix coating, cell adhesion time, cell inoculation density, flow rate) was not successful in the 2D biochip culture. We proposed a second strategy using 3D spheroids created from honeycomb static cultures. Spheroids in static experiments carried out over 14 days demonstrated that they expressed high levels of β-cell markers (*INS* mRNA) and higher α-cell markers (*GCG* mRNA and glucagon positive staining), when compared to Petri 2D cultures. Furthermore, the 3D spheroids were specifically able to secrete insulin in response to both high/low glucose stimulation and GLP1 exposure. The spheroids were successfully inoculated into biochips and maintained for 10 days in perfusion. The 3D biochip cultures increased mRNA levels of *GCG* and maintained high levels of β-cell markers and responsiveness to both high/low glucose and GLP1 stimulation. Finally, C-peptide and insulin secretion were higher in biochips when compared to static spheroids. These results illustrate the promising potential for hiPSCs derived β-cells and their spheroid-based pancreas-on-chip model for pancreatic disease/diabetes modeling and anti-diabetic drug screening.

Keywords: human induced pluripotent stem cells, β-pancreatic cells, microfluidic culture, 3D spheroids.

Introduction

In 2019, the International Diabetes Federation (IDF) reported that 466 million people worldwide (9.3 % of adults aged 20-79 years) have diabetes mellitus (DM) (IDF Diabetes Atlas, 2019). The predictions for DM are worrying, with 700 million people affected (10.9% of the population) by 2047 (IDF Diabetes Atlas, 2019). The annual healthcare cost of diabetes was estimated at approximately 760 billion USD in 2019 and is predicted to reach 800 billion USD by 2040 (IDF Diabetes Atlas, 2019; Rogal et al., 2019). There are two main types of DM: type 1 DM (T1DM, 5-10 % of diabetic patients) and type 2 DM (TD2M, more than 90% of cases, Essaouiba et al., 2020). T1DM results from autoimmune destruction of pancreatic islet beta cells leading to a lack of insulin secretion (Jellali et al., 2020; Rogal et al., 2019). The standard practice for T1DM treatment is daily scheduled or continuous insulin administration, based on monitoring of glucose levels (Galderisi et al., 2017). T2DM is caused by the insensitivity of target tissues to insulin and impaired insulin secretion (DeFronzo et al., 2015). T2DM can be managed by lifestyle adjustments and oral antidiabetic agents such as thiazolidinediones, metformin, sulphonylureas, meglitinides and GLP-1 receptor agonists (Kahraman et al., 2016).

For both types of DM, there is a real need to develop relevant models for cell therapy, investigation of the underlying mechanisms in diabetes and the etiology of beta cell dysfunction, and anti-diabetic drug screening. Several animal models (in particular rodents) with the characteristics of T1DM and T2DM have been used for DM studies (King and Bowe 2016). However, animal models have their limitations because of species differences, resulting in poor extrapolation from animal research to human (Cota-Coronado et al., 2019; Merlier et al., 2017). With the development of tissue-engineering 3D cultures, dynamic organ-on-chip cultures, and co-culture models, *in vitro* cell-based models have the potential to mimic the *in vivo* physiological microenvironments of organs and provide relevant models for diabetes modelling. The type of cells and their source are a key factor for the development of *in vitro* models (Rogal et al., 2019). Primary human β-cells or islets are considered a gold standard for *in vitro* models in DM research (Kaddis et al., 2009). However, the

limited availability, the high cost of islet isolation and inter-donor differences remain major limitations to using primary islets/β-cells (Balboa et al., 2019; Amirruddin et al., 2020). Furthermore, primary islets rapidly lose their specific functions when cultured *in vitro* (Rogal et al., 2019). β-cell lines are a potential alternative to primary β-cells as they have an infinite life span, low cost and have reduced variability (Scharfmann et al., 2019). Nevertheless, these cells have limited functionality, lack plasticity and there are differences in the gene expression of β-cell markers when compared to primary cells (Amirruddin et al., 2020; Bakhti et al., 2019).

In 2007, Takahashi et al., achieved a major breakthrough by reprogramming patient somatic cells into human induced pluripotent stem cells (hiPSCs) (Takahashi et al., 2007). The availability of these cells, along with their ability to both self-renew indefinitely *in vitro*, and generate different cell types, provide great insight for investigating the pathogenic mechanisms of diseases and for contributing to cell therapies and drug development (Balboa et al., 2019; Amirruddin et al., 2020). Furthermore, unlike human embryonic stem cells (hESCs), hiPSCs do not raise any ethical problems and offer the possibility of developing patient-specific models (Balboa et al., 2019). hiPSC differentiation into mature selected tissue is a strategy based on translational embryology (Spence *et al.*, 2007). This sequential process makes it possible to direct the hiPSCs from the endoderm stage to specific cell types, such as β-cell pancreatic progenitors and as far as pancreatic β-like cells. In light of this, several protocols following this philosophy have been proposed (Hosoya, 2012; Zhu et al., 2016). While it was demonstrated that partially functional pancreatic β-cell tissue could be achieved, attaining levels of maturity and functionality comparable to those of the *in vivo* situation is still challenging. Nevertheless, it is reported that iPSC derived pancreatic cells may be a source of cells for pancreatic disease models (Kahraman et al., 2016; Hohwieler et al., 2019).

Organ-on-chip is one of the more promising techniques for investigating complex human diseases that allow human physiological *in vitro* responses (Esch et al., 2015). These microfluidic platforms improve the exchange and transport of nutrients, oxygen, metabolic waste and hormones, and create “physiological-like” situations such as cell-cell interaction, shear stress and chemical gradients (Merlier et al., 2017; Rogal et al., 2019). Several previous studies have reported that perfused

microfluidic cultures enhance the long-term viability and functionality of pancreatic islets and β-cell spheroids (Jun et al., 2019; Bakhti et al., 2019). Last but not least, organ-on-chip technology makes possible the co-cultures of two or more organs in separate micro-bireactors, connected by soluble factors exchanged through the microfluidic network (Merlier et al., 2107). This system can be used to study inter-organ crosstalk such as interactions between pancreatic islets and hepatic cells (Bauer et al., 2019; Essaouiba et al., submitted). The co-culture of two or more organs is a powerful tool for modulating multi-organ diseases such as diabetes. Although organ-on-chip technology has been used to reproduce *in vitro* pancreas-on-chip models using pancreatic islets or β-cell spheroids (Jun et al., 2019; Lee et al., 2018; Li et al., 2017; Mohammed et al., 2009; Bauer et al., 2017; Schulze et al., 2017; Zbinden et al., 2020), only very few studies have already coupled iPSC derived pancreatic-like cells with organ-on-chip technology (Rogal et al., 2019; Hirano et al., 2017; Tao et al., 2019).

Our group has developed organ-on-chip technology contributing to investigations into human liver metabolism (Prot et al., 2011; Jellali et al., 2016), the human liver regeneration process (Danoy et al., 2019), as well as crosstalk and synergy between different organs such as the liver's interaction with the intestine and kidneys (Bricks et al., 2014; Choucha-Snouber et al., 2013). Recently, we have investigated the behavior of rat islets of Langerhans and their interaction with hepatocytes in microfluidic biochips (Essaouiba et al., 2020; Essaouiba et al., submitted). In this paper, we propose extending those microfluidic developments to pancreatic human β-cells derived from induced pluripotent stem cells. We investigated and compared several protocols for biochip cultures, as well as 2D and 3D culture configurations.

2. Material and methods

2.1. Cell source

The cells used in this work (Cellartis hiPSCs derived β-cells) were provided by Takara Bio (Japan). Cellartis hiPSC beta cells were differentiated from ChiPSC12

lines and provided in stage 1 of maturation (Fig.1). The hiPSCs derived β-cells were differentiated into insulin-producing cells using the hiPSCs beta cell media kit (cat. N° Y10108, Takara Bio, Japan), according to the manufacturer's instructions.

2.2. 2D Petri pancreatic β–cell culture protocol

Culture dishes (24-well plates) were coated with a Cellartis beta cell coating (cat. N° Y10103) and incubated at 37°C. After 1h, the coating solution was removed and 500 µL of maintenance culture medium (Cellartis beta cell basal medium Y10104, supplemented with beta cell supplement Y10102) containing cells were added to each well. The cells were inoculated at a density of $2x10^5$ cells/cm^2 and the plates incubated at 37°C in an atmosphere supplied with 5% CO_2. The maintenance culture medium was used for 12 days and changed every day. The assay medium (Cellartis beta cell medium 2 Y10105, supplemented with beta cell supplement Y10102) was then used from day 12 to day 15 (Fig.1).

2.3. 3D spheroid cultures using honeycomb technology

To create the spheroids, we used the honeycomb technology previously developed by Shinohara et al., 2014, 2017. Briefly, the honeycomb polygons were made of PDMS and had the geometric characteristics of 126 µm in width and 129 µm in depth (Fig.2A). The PDMS honeycomb sheet was seeded on to a bottomless 24-well plate. Each well of the 24-well plate contained 6750 honeycombs. The plates were sterilized with ethanol for one hour, coated with pluronic-PBS solution overnight (Pluronic® F-127 Sigma) and rinsed three times with phosphate-buffered saline (PBS, Gibco) and once with maintenance culture medium. After thawing, the β–cells were dropped into the honeycomb in 500 µL of maintenance medium and incubated at 37°C in an atmosphere supplied with 5% CO_2. Two densities were tested: $2x10^5$ cells per well (low-density, LD) and $6x10^5$ cells per well (high-density, HD). The sequence of the culture medium change was exactly the same as the 2D Petri monolayer cultures. Nevertheless, after 24h, the medium was adjusted to 1 mL. We then removed 600 µL at each culture medium change, replacing them with 600 µL of fresh

medium (thus resulting in there always being 400 μL in the honeycombs to prevent the spheroids suction).

2.4. Dynamic cultures in biochips

We tested two biochip culture strategies. The first was a “2D monolayer”, where cells adhered to the surface culture inside the biochip. The second strategy consisted of the dynamic culture of 3D β-cell spheroids.

2.4.1. Microfluidic biochip manufacture

In the 2D culture, the biochip consisted of a cell culture chamber manufactured with two polydimethylsiloxane (PDMS) layers. The microstructured bottom layer, with series of microchambers and microchannels (depth of 100 μm, Fig.2B), was used as a support for cell attachment. The second layer, with a reservoir (depth of 100 μm), was placed on top of the first layer and included an inlet and outlet microfluidic network for homogenous culture medium distribution (Fig.2B). The design and dimensions of the biochip were described in our previous work (Baudoin et al., 2011; Jellali et al., 2016). For the 3D β-cell spheroid cultures, construction of the biochip included a first PDMS layer (bottom layer) for trapping islets, which contained a series of crescent-shaped structures of 600 μm in diameter (height of 300 μm), and spaced 300 μm apart (Fig.2B). The second PDMS layer (top layer) was the same as described above for 2D biochip.

The biochips were made of PDMS using the conventional replica molding process. The mold masters for the bottom and top layer of the biochips were manufactured using photolithography with SU-8 photosensitive resin. The PDMS prepolymer (Sylgard 184, Dow Corning in a mixture of 10:1 base polymer: curing agent) was poured on to the SU-8 master and cured for 2 h at 75°C. The surfaces of the PDMS layers obtained were activated with reactive air plasma (1 min; Harrick Scientific) and brought together immediately to form an irreversible seal.

2.4.2. Biochip cultures

Before the cell experiments, the biochips and perfusion circuits (silicone tubing and bubble trap) were sterilized by autoclaving and dried in an oven. Then, the biochips were assembled with the perfusion system and filled with culture media in order to remove the air bubbles and moisturize the circuits. The bubble trap was used as a reservoir interconnected to the biochips by the silicone/Teflon tubing with a diameter of 0.65 mm. The assembled experimental setup (biochip, tubing, reservoir, and peristaltic pump) is presented in Fig.S1 (supplementary file).

The protocol for 2D cultures in biochips was similar to the protocol used in 2D Petri cultures (section 2.2). In this protocol, the biochips were coated using the extracellular matrix solution provided in the β-cell kit (Cellartis beta cell coating, cat. N° Y10103) and incubated at 37°C. Then, several parameters were tested to establish the best attachment protocol as shown in Table S1 (supplementary file). It included modulation of the inoculation cell density, incubator oxygen concentration, composition of the culture medium, and time of adhesion before perfusion. In 3D biochip cultures, the β-cell spheroids were formed using the honeycomb technology as described in the section above. After 4 days of culture in the honeycombs, the spheroids formed were collected and seeded in biochips (Fig.1). In order to minimize any spheroids damage, wide orifice pipette tips with low binding were used during the entire handling process. After spheroids seeding, the biochips were incubated at 37°C in a 5% CO_2 supplied incubator for 1h to allow the crescent-shaped structures to trap the spheroids. The biochips were then connected to the perfusion circuits and peristaltic pump, and the perfusion started at 20 µL/min. The entire setup was continuously incubated at 37°C in a 5% CO_2 supplied incubator. A similar protocol was used in 3D spheroid honeycomb static cultures for comparative purposes. For that purpose, the spheroids formed (after 4 days of culture in the honeycombs) were collected and seeded in a new honeycomb plate (using the same density as the biochip). The culture medium change sequence was the same as for the 2D Petri monolayer cultures and 3D static cultures.

2.5. RTqPCR assays

Total RNAs were extracted and purified from samples using a hybrid protocol that combined Trizol™ Reagent (Life Technologies) and the RNeasy Mini Kit

(QIAGEN 74104) following the manufacturer's instructions. The concentrations and qualities of the RNAs extracted were assessed using a BioSpec-nano (Shimadzu Scientific Instruments). Reverse-transcription into cDNA was performed from 0.5 µg of total RNA using the ReverTra Ace qPCR RT Master Mix with gDNA Remover (TOYOBO). Real-time quantitative PCR was then performed with the THUNDERBIRD SYBR qPCR Mix (TOYOBO) according to the manufacturer's protocol and a StepOnePlus Real-Time PCR system (Applied Biosystems). Primer sequences of genes are shown in Table S2 (supplementary file). β-Actin was used as the reference gene.

2.6. Immunostaining

After transfer to an untreated TCPS 24-well plate, the spheroids were washed with phosphate buffer saline solution (PBS) and fixed in paraformaldehyde 4% at 4°C overnight. In order to perform the immunohistochemistry (IHC) staining in a 3D structure, the spheroids were permeabilized with 1% Triton X100 in PBS for 3 hours at 4°C and washed 3 times with PBS for 30 min. Then, the spheroids were blocked with a gelatin buffer for 24 hours at 4°C. Primary antibodies (Table S3, supplementary files) were incubated for 24 hours at 4°C in a BSA/PBS solution. After washing with PBS, secondary antibodies (Table S3, supplementary files) were further incubated overnight in a BSA/PBS solution at 4°C in the dark. Finally, the nuclei were stained with DAPI (342-07431, Dojindo) at 1/1000 for 30 min at room temperature (RT) in the dark. All the incubations and washing steps were carried out using a shaker. Observations were made using an Olympus IX-81 confocal laser-scanning microscope.

The IHC staining of the 2D monolayer β-cells followed a similar protocol in which the period of permeabilization, first antibody incubation and second antibody incubation were reduced to 15 min at RT, overnight at 4°C, and 2 hours at RT, respectively. The primary and secondary antibodies used are listed in Table S3 (supplementary file).

2.7. Insulin and C-peptide measurements

The insulin and C-peptide released into the culture medium from the different culture conditions were assessed using ELISA assays, following the manufacturer's protocol. The following kits were used: insulin (human insulin ELISA kit, 10-1113-01, Mercodia) and C-peptide (human C-peptide ELISA kit, 10-1136-01, Mercodia). The results were obtained using an iMark microplate reader (Bio-Rad, Osaka, Japan) set to a wavelength of 450nm.

2.8. Insulin secretion by low / high glucose assays

At the end of the cultures, we carried out a low / high glucose stimulation to check insulin production. In the biochips, the culture medium was removed from the bubble trap, and the perfusion circuits with the culture chamber containing the spheroids were washed with a 0-glucose solution (DMEM, No Glucose, Wako) for 2 hours. Then, the washing 0-glucose solution was removed from the bubble trap and 1 mL of fresh 0-glucose was added and perfused for 2 additional hours. After this low glucose perfusion, the spheroids were exposed to a high glucose culture medium for 2 hours (25 mM of glucose; DMEM, 25 mM high Glucose, Wako). This involved the low glucose solution being removed from the bubble trap, replaced with 1mL of high glucose solution and the perfusion launched for 2h. In the Petri dishes (2D and 3D spheroids), this protocol led to 2h 0-glucose exposure (washing), followed by another 2h 0-glucose exposure and finally 2h of high glucose stimulation. At the end of the assays, basal media were re-established for all conditions.

2.9. Glucagon-like peptide-1 (GLP1) stimulations

In order to test the response of the β–cells to drug stimulations, we exposed the cultures to GLP1. To do so, we added 100 nM of GLP1 to the culture medium for the last 24h of culture, on day 13, until day 14. This provided 24h of exposure to the drug.

2.10. Statistical analysis

All experiments were repeated at least three times. The data are presented as the mean ± standard deviations (SD) of 9 biochips (3 biochips from 3 different experiments, n=3x3). The data were analyzed statistically using GraphPad prism 8 software (San Diego, USA). The Kruskal Wallis test was performed to determine any significant differences between the samples (P values < 0.05 were identified as statistically significant).

3. Results

3.1 The 2D monolayer strategy derived β-cells in Petri dishes but failed in biochips

The protocol recommended by Cellartis (cells plated in Petri 2D) led to successful cells adhesion and 16 days of cell culture (Fig.3 A-C). The β-cells profile, at the protein level, was confirmed by the expression of PDX1, MAFA and insulin, as demonstrated by the immunostaining in Fig.3 D-G. The RTqPCR analysis illustrated successful β-cells differentiation in Petri dishes, as demonstrated by the upregulation of the mRNA levels of *INS*, *PDX1*, *NGN3*, *NKX6.1* and *NKX2.2* at the end of the differentiation, when compared to the first day of culture and to the iPSCs standard (Fig.3H). Finally, the functionality of the cells was confirmed by the secretion of the C-peptide (Fig.3I). Secretions reached 4.5±0.5 pmol/10^5 of inoculated cells (8600 pmol/L/10^5 cells). The β-cells culture was also responsive to high / low glucose stimulation, leading to a 2.6±0.9 (n=4 assays) times more insulin secretion in high glucose stimulation when compared to low glucose stimulation (data not shown). Finally, glucagon production was not detected (either by ELISA, or by immunostaining, data not shown). This set of results confirmed that the β-cells differentiated in 2D Petri conditions.

The same strategy was investigated in the biochips by directly seeding the hiPS β-cells, after thawing, inside the 2D biochips. To try to attach the cells to the bottom surface of biochips, we investigated several conditions including (i) the extracellular matrix coating; (ii) the presence of a rock inhibitor in the seeding medium; (iii) adjusting oxygen concentrations during the adhesion phase; (iv) and the

density of the seeded cells. The complete set of parameters tested is summarized in Table S1 (supplementary file). After 24h of adhesion, the cells were not able to attach in most of the conditions tested. The typical morphology is presented in Fig.4A (24h after seeding, ↓ density). When using the high cell density, few cells managed to attach but they quickly formed aggregates, as shown in Fig.4A (24h after seeding, ↑ density). Then, once the perfusion was launched, the cells were detached after 5h of culture (Fig.4A, 5h after perfusion, ↑ density). Finally, no optimized condition was found to make successful 2D monolayer biochip cultures possible (n=3 cryotubes used in 3 independent experiments, leading to 26 biochips).

3.2 3D spheroid strategy in static honeycombs

As the biochip cultures failed with the monolayer of β-cells, we cultured the cells into spheroids to create aggregates and allow us to seed them in the biochips with crescent-shaped microstructures. The 3D spheroids were created using honeycomb microwells. Two cell densities, $0.6x10^6$ and $0.2x10^6$ cells per well, were tested (Fig. 4 B). The aggregates were formed after 7 hours of culture but still presented a rough circumference (Fig.4B, 7h after seeding). They started to present a round shape after 3 to 4 days of culture. The highest density led to spheroids of 90±15 μm in diameter (Fig.4B, 14 days). The lowest density led to smaller spheroids, of 50±25 μm in diameter, but with greater dispersion (Fig.4B, 14 days). Based on the number of honeycombs (6750), we estimated about 30 and 90 cells/spheroid in low- and high-density, respectively.

The immunostainings are presented in Fig.5 for both types of spheroid. They confirmed that the spheroids were positive for β-cell markers: insulin, MAFA and PDX1. When compared to 2D cultures, the spheroids appeared to be positive for glucagon (in both high- and low-density).

The β-cells spheroids led to positive C-peptide secretion, as shown in Fig. 6 A. When normalized by the number of seeded cells, we found that the secretion of C-peptide was similar in both high- and low-density experiments (Fig.6A). Peak concentrations of around 5 pmol/10^5 inoculated cells were achieved after 13 days of

culture. Furthermore, at the end of the experiment (day 14), we detected higher secretion of insulin in the low-density spheroids cultures (210±65 pmol/10^5 cells) when compared to the high-density spheroids cultures (98±20 pmol/10^5 cells), as shown in Fig.6B. Both culture modes were responsive to the high/low glucose stimulations (Fig.6C). Namely, the high glucose stimulation led to 4.5±1.3 times more insulin production when compared to the low glucose condition in high-density spheroids (GSIS index). In the low-density spheroid cultures, the GSIS index was 11.5±5. Finally, both types of spheroid were also responsive to GLP1 drug stimulation, leading to double the insulin secretion (Fig.6D). The ratios of insulin secretion (GLP1 treated/control) were 1.96 and 1.6 in high- and low-density, respectively.

3.3. Critical transfer of 3D β-cells spheroids into microfluidic biochips

After 4 days of culture in the honeycomb, once the spheroids had presented a round shape, they were collected and inoculated into the 3D biochips. The low-density spheroids were very fragile, and we were not able to collect the spheroids without damaging them (loss during pipetting, loss during centrifugation, spheroids destroyed during handling, n=6 honeycomb microwell dishes were tested for transfer). As a result, we only transferred the high-density spheroids into the biochips.

Although it was possible to inject the high-density spheroids, we still noticed significant loss: we counted only 150±50 spheroids entering the biochips. As we used one honeycomb Petri to fill 6 biochips, this led to about 82% - 91% of spheroids lost (600/6750 – 1200/6750, this will be discussed below). The perfusion was started for 10 additional days, leading to 14 days of culture (4 days in static conditions to create the spheroids and 10 days of dynamic culture). At the end of the perfusion, we confirmed the presence of the spheroids (number similar to the inoculation density, about 160±66 spheroids), illustrating successful perfusion culture as shown by their morphologies, which are presented in Fig.4C.

3.4. High functionality of the 3D pancreatic spheroids in microfluidic biochips

Analyzing the mRNA levels revealed major modifications to the profile of the cells when we compared the 2D Petri, 3D Petri honeycomb (3D-HD) and the 3D biochip cultures (Fig.7). The spheroid culture, in 3D Petri, appeared to increase the gene expression of β-cell markers such as *PDX1*, *NKX2.2*, *NKX6.1* and *INS* (Fold change, FC of 3.3, 2.6, 3 and 3.8, respectively when compared to Petri 2D). In parallel, alpha or delta cell markers such as *GCG* (FC 2.6), *SST* (FC 6.6) and glucose transporter *GLUT2* (FC 19) were higher in static 3D spheroid conditions than in 2D Petri conditions. Finally, *GCK, UCN3* and *NGN3* were downregulated in static 3D spheroids (in comparison with Petri 2D).

Once cultivated in the biochip, we found an increase in mRNA levels of alpha cells markers (*GCG*, FC 6.8), delta cell markers (*SST*, FC 3.5) and glucose metabolism markers (*GLUT2*, FC 12.7), when compared to 2D cultures (Fig.7). Furthermore, we found clear upregulation of *GCG* when compared to the 3D Petri cultures. Although β-cells markers such as *NKX6.1* and *NKX2.2* were 2.5-2.7 times higher in the biochips when compared to 2D (and similar to 3D Petri levels), the levels of *PDX1* and *INS* mRNA were similar in the 2D cultures and biochips. Finally, *MAFA* (FC 0.42), *GCK* (FC 0.11), *UCN3* (FC 0.12) and *NGN3* (FC 0.08) were lower in the biochips, when compared to 2D cultures.

Immunostaining confirmed that the spheroids cultures in biochips expressed typical β-cells markers, as illustrated by the detection of insulin, MAFA and PDX1 positive cells (Fig.5A). However, we also found cells positive for glucagon, demonstrating the presence of alpha-like cells as well. As mentioned above, in the 2D Petri cultures, we never detected glucagon positive cells.

The kinetics of C-peptide secretion in biochips presented in Fig.8A demonstrates the functionality of the spheroids. To be able to compare the dataset in biochips and honeycombs (3D-HD), we normalized by number of spheroids at the end of the experiments. When normalized by the number of spheroids, C-peptide secretion in the biochips was measured at around 0.02-0.05 pmol/islet between day 9 and the end of the perfusion (day 14, Fig.8A). Furthermore, we detected higher quantities of C-peptide in biochip cultures when compared to 3D honeycombs (about

10-30 times higher). We also observed higher secretions of insulin in the biochip spheroids cultures when compared to the static spheroids cultures (3D-HD), as shown in Fig.8B. Insulin secretion was about 2.55 times higher in the biochips at the end of the experiment (day 14).

The functional assays performed using high/low glucose stimulation (glucose-stimulated insulin secretion, GSIS) and GLP1 stimulation demonstrated that the biochip spheroids were able to adapt their insulin response, as shown in Fig.8C and 8D, respectively. However, in terms of the induction ratio itself, no difference between the biochip and the static honeycomb cultures was observed. The GSIS index (glucose-stimulated insulin secretion: insulin measured in high-glucose divided by insulin in low-glucose) values were of 3.2±1.1 and 4.5±1.2 in the biochip and static honeycomb, respectively (Fig.8C). Concerning the GLP1 effect, the levels of insulin were 1.5 (static spheroids) and 2 (biochip spheroids) times higher after GLP1 stimulation, when compared to the control (Fig.8D).

Discussion

In this work we investigated the behaviors of pancreatic β-cells derived from human induced pluripotent stem cells. The 2D cultures in Petri dishes confirmed the functionality of the derived tissue as a pancreatic-like β-cells. This was illustrated by C-peptide production, the positive staining for insulin, negative staining for glucagon, and insulin secretion in response to low/high glucose stimulation. Other 2D protocols for iPSCs derived pancreatic β-cells, including different growth factor sequences, iPS cell lines and sources, have also reported successful insulin and C-peptide functional tissues (Yabe et al., 2017; Southard et al., 2018; Pelligrini et al., 2018). Those works attained C-peptide production of up to 5000 pmol/L/2x10^6 cells after 23 days of culture (Yabe et al., 2017), and ranging from 700 to 1500 pmol/L/6.4x10^4 of plated cells after 28 days of culture (Southard et al., 2018). Our differentiation took place over 16 days after stage 1 of the Cellartis protocol (Fig 1), corresponding to 37 days overall of differentiation from undifferentiated iPSCs. As we reached a peak of 8600 pmol/L/10^5 of plated cells (4.5 pmol/10^5 of cells) after 35 days, our results appeared consistent with the data in the literature.

Although the 2D Petri cultures were encouraging, we failed to create 2D cultures of β-cells in our microfluidic devices (our primary goal). This strategy was first investigated because the Cellartis ChiPSC12 kit is recommended for use in monolayers. We could not identify the key parameters leading to this failure. First the cell adhesion, and then the cell monolayer could not be created in the biochips even though we tested several conditions, including the initial cell density, extracellular matrix coating and oxygen adhesion conditions (see Table S1, supplementary file). Several hypotheses can be formulated: (i) the first is related to choosing the extracellular matrix and its protocol of coating on PDMS. PDMS is a hydrophobic material that needs an appropriate coating of ECM to make cell adhesion possible. The Cellartis recommended ECM, when coated on PDMS, may require higher concentrations of ECM compounds and longer incubation times on the surface compared to the recommended protocol for polystyrene Petri cultures; it may also require other components, such as Matrigel (suitable for iPSC hepatocytes on PDMS for instance, Danoy et al., 2019) (ii) in addition, during the adhesion phase of cells in biochips, and the first hours of perfusion, our previous experiments (with cell lines) demonstrated that there was significant glucose consumption by the cells (Prot et al., 2011). As the biochip volume was 30 μL, leading to a cell/volume ratio of 6 600 000 cells/mL in the biochip (200 000 cells/cm^2 in 30 μL) and 400 000 cells/mL in Petri dishes (200 000 cells/cm^2 in 0.5 mL), we can hypothesize that there was a local shortage of a critical nutrient at the density inoculation tested. In this context, several reviews to help obtain successful microfluidic cultures have been proposed in the literature, exploring other 2D strategies (Yu et al., 2007, Young and Beebe 2010); (iii) we also previously reported some ROS production during the adhesion stage of cell culture in a microfluidic environment and during the first hours of perfusion (Leclerc et al., 2015). To avoid potential apoptosis, we tested the effects of a ROCK inhibitor, as it is used in several iPSC protocols during the plating stage after thawing (Emre et al., 2010; Watanabe et al., 2007), but it did not lead to improved adhesion. As a result, more extensive investigations are needed to solve the issues with the 2D biochip cultures.

As an alternative to the 2D biochip culture strategy, we proposed a 3D spheroid protocol. In honeycomb static cultures, our spheroid protocol contributed to generating β-cells-based spheroids secreting C-peptide and insulin. We found that low cell density spheroids generated smaller spheroids (50 µm) compared to high cell density ones (100 µm), although they produced similar levels of C-peptide. The effects of cell density and spheroid diameter on functionality were documented with β-cells line (Shinohara et al., 2014; Bernard et al., 2012). Microwells of 100 to 300 µm in diameter led to insulin levels close to 75ng/1000 cells in Min-6 (Bernard et al., 2012). In our honeycomb geometry, previous works with Min-6 spheroids ranging from 60 to 150 µm in diameter produced levels of insulin close to 60 ng/ng-DNA (Shinohara et al., 2014). Furthermore, *in vitro* secretion of insulin from derived iPSCs β-cells spheroids is reported as ranging from 1.6 to 2 µUI/10^3 cells (Millman and Pagliuca 2017; Pagliuca et al., 2014, Millman et al., 2016). Based on the data in Figs. 6 and 8, our study contributed to generating β-cell-based spheroids secreting insulin around 1.8 µUI/10^3 cells in the high density spheroids used in 3D Petri (with a conversion of 0.144 µUI/mL = 1 pmol/L). Finally, insulin secretion stimulated by high glucose in primary human islets led to 4-fold induction (glucose 5.6 mM), 16-fold (16.7 mM) after one hour of exposure (Mc Donald et al., 2011) and about 10-fold at 11 mM, 20 min of stimulation (Pelligrini et al., 2018). These results appear to be in the range of our data in which the mean value of the induced insulin secretion ratio was close to 4 and 11 in the 3D high- and low-density spheroids, respectively.

We then successfully applied our 3D spheroid cultures to the microfluidic biochips. There was still a significant loss of spheroids, and a third strategy consisting of generating the islets inside the biochips, to avoid having to transfer them, needs to be investigated. Nevertheless, thanks to the biochips, we were able to improve spheroid functionality when compared to 3D Petri controls in terms of insulin and C-peptide secretion. The enhancements of basal pancreatic islets or pseudo-islets functions such as insulin secretion and glucose-induced insulin secretion under microfluidic flow have been observed consistently in the literature (Jun et al., 2019; Tao et al., 2019; Li et al., 2013; Sankar et al., 2011). We suspect that changing the continuous culture medium played a part in continuously stimulating the spheroids with high glucose stimulation, and thus insulin secretion.

The spheroids in the biochip cultures were also responsive to both low/high glucose stimulation and GLP1 exposure.

Focusing on the 3D spheroids experiments, we found that the 3D spheroids had greater heterogeneity (in the 3D Petri and 3D biochip conditions), when compared to the Cellartis optimized 2D protocol. The mRNA levels and immunostaining analysis revealed partial loss of the β-cell specifications in the 3D spheroids, and the potential orientation toward pancreatic α-cells and δ-cells sub-lineages. This was illustrated by the positive staining of the glucagon, upregulation of *SST* and *GCG,* and downregulation of *NGN3* in the spheroids in 3D conditions. It is reported in the literature that *PDX1*, *MAFA*, *NGN3* and *NKX6.1* play a pivotal role in β-cells differentiation, as well as in various processes within α-cell differentiation (Schaffer et al., 2010; Matsuoka et al., 2017; Zhu et al., 2016; Brissova et al., 2018). Furthermore, the *SST* gene (upregulated in the 3D Petri and 3D biochip cultures when compared to 2D Petri) is a key player in δ-cell specification (Hauge Evans et al., 2009).

In parallel, modification to the differentiation pattern was concomitant with high levels of *GLUT2* and *GCG*, and low levels of *GCK* in 3D cultures. We confirmed the high level of glucose in the culture medium, even in 3D Petri and 3D biochip cultures (in the culture medium from step 2, we measured 9.5±0.5 mM, data not shown). As a result, we can hypothesize that the secretion of glucagon in the spheroids (detected by positive immunostaining) is due to local shortage of glucose inside the spheroid, and thus to a modulation of glucose transport inside the spheroid (*nb:* it has been reported that *GLUT2* is weakly expressed in β-cells and over-expressed in α-cells, leading to the way the glucose is transported being modulated, but not the fact of the transport itself, Heimberg et al., 1995). *GCK* is a glucose sensor that regulates insulin release in β-cells, and glucose homeostasis in α and δ-cells (Matschinsky et al., 2019). In addition, *GCK* governs an α-cell metabolic pathway by suppressing glucose-related secretion of glucagon at/or above normoglycemic levels (Basco et al., 2018). Downregulation of *GCK* in our 3D cultures appeared consistent with glucagon secretion due to glucose shortage in the center of the spheroids. As a result, in agreement with pancreas organogenesis (Puri et al.,

2015), our data suggest that there is major cell plasticity in the differentiation process of the present iPSCs in response to the 3D spheroid culture conditions. Additional investigations are now required to understand these phenomena. More particularly, it would be interesting to see whether complex physiological islet differentiation into multicellular pancreatic lineages including α,β and δ cells can occur in these 3D spheroid microfluidic cultures.

Conclusion

In summary, we investigated the behaviors of β–cells derived from hiPSCs in various culture conditions. 2D monolayer cultures generated typical β–cells profiles, as shown by C-peptide production and undetected glucagon secretion. When cultivated in 2D biochips in a monolayer, we did not find any stable protocol making their microfluidic cultures possible. When the cells were cultivated in 3D spheroids, the cells presented higher heterogeneity, as seen in the appearance of α, β and δ-cell markers at the mRNA level, and glucagon positive immunostaining, in addition to the secretion of C-peptide. The 3D spheroids were then successfully cultivated in a 3D biochip under microfluidic conditions. The microfluidic culture established contributed to increasing pancreatic maturation by improving C-peptide and insulin secretion levels. The high level GLUT2 and low level GCK in 3D static spheroids and 3D biochips, when compared to 2D Petri, suggested modulation of glucose metabolism and transport as a potential regulator of pancreatic specification during differentiation into 3D spheroids and 3D biochips. We believe that our results are encouraging for the development of functional pancreas-on-chip in vitro models using the advantages of organ-on-chip technology and hiPS cells, a promising source of cells.

Acknowledgements

Part of this project was funded by the French National Research Agency (ANR-16-RHUS-0005). We thank Tokito Fumiya for his help with manufacturing the honeycombs. We thank Laurent Mazenq and the LAAS Renatech platform for the mold master used to manufacture the crest 3D biochips. Amal Essaouiba received PhD funding from the French Ministry of Higher Education and Research, mobility

grants from CNRS/IIS LIMMS UMI 2820 and from the Université de Technologie de Compiegne.

Conflict of interest

The authors declare no conflict of interest.

References

Amirruddin, N.S., Low, B.S.J., Lee, K.O., Tai, E.S., Teo, A.K.K.,2020. New insights into human beta cell biology using human pluripotent stem cells. Semin. Cell Dev. Biol. 103, 31-40. https://doi.org/10.1016/j.semcdb.2019.11.004.

Bakhti, M., Böttcher, A., Lickert, H., 2019. Modelling the endocrine pancreas in health and disease, Nat. Rev. Endocrinol. 15, 155-171. https://doi.org/10.1038/s41574-018-0132-z.

Balboa, D., Saarimäki-Vire, J., Otonkoski, T., 2019. Concise Review: Human Pluripotent Stem Cells for the Modeling of Pancreatic β-Cell Pathology. Stem Cells. 37, 33-41. https://doi.org/10.1002/stem.2913.

Basco, D., Zhang, Q., Salehi, A., Tarasov, A., Dolci, W., Herrera, P., Spiliotis, I., Berney, X., Tarussio, D., Rorsman, P., Thorens, B., 2018. α-cell glucokinase suppresses glucose-regulated glucagon secretion. Nat. Commun. 9, 546. https://doi.org/10.1038/s41467-018-03034-0.

Baudoin, R., Griscom, L., Prot, J.M., Legallais, C., Leclerc, E., 2011. Behaviour of HepG2/C3a cell culture in a microfluidic bioreactor. Biochem. Eng. J. 53, 172-181. https://doi.org/10.1016/j.bej.2010.10.007.

Bauer, S., Wennberg Huldt, C., Kanebratt, K., Durieux, I., Gunne, D., Andersson, S., Ewart, L., Haynes, W., Maschmeyer, I., Winter, A., Ämmälä, C., Marx, U., Andersson, T., 2017. Functional coupling of human pancreatic islets and liver spheroids on-a-chip: Towards a novel human ex vivo type 2 diabetes model. Sci Rep. 7, 14620. https://doi.org/10.1038/s41598-017-14815-w.

Bernard, A., Lin, C., Anseth, K., 2012. A microwell cell culture platform for the aggregation of pancreatic β-cells. Tissue Eng. Part C Methods. 18, 583-592. https://doi.org/10.1089/ten.TEC.2011.0504.

Bricks, T., Paullier, P., Legendre, A., Fleury, M.J., Zeller, P., Merlier, F., Anton, P.M.,

669 Leclerc, E., 2014. Development of a new microfluidic platform integrating co-
670 cultures of intestinal and liver cell lines. Toxicol. in Vitro. 28, 885-895.
671 https://doi.org/10.1016/j.tiv.2014.02.005.
672 Brissova, M., Haliyur, R., Saunders, D., Shrestha, S., Dai, C., Blodgett, D.M., Bottino,
673 R., Campbell-Thompson, M., Aramandla, R., Poffenberger, G., Lindner, J., Pan,
674 F.C., von Herrath, M.G., Greiner, D.L., Shultz, L.D., Sanyoura, M., Philipson,
675 L.H., Atkinson, M., Harlan, D.M., Levy, S.E., Prasad, N., Stein, R., Powers, A.C.,
676 2018. α cell function and gene expression are compromised in type 1 diabetes.
677 Cell rep. 22, 2667-2676. https://doi.org/10.1016/j.celrep.2018.02.032.
678 Choucha-Snouber, L., Aninat, C., Grsicom, L., Madalinski, G., Brochot, C., Poleni,
679 P.E., Razan, F., Guguen Guillouzo, C., Legallais, C., Corlu, A., Leclerc, E.,
680 2013. Investigation of ifosfamide nephrotoxicity induced in a liver–kidney
681 co-culture biochip. Biotechnol. Bioeng. 110, 597-608.
682 https://doi.org/10.1002/bit.24707.
683 Cota-Coronado, A., Ramírez-Rodríguez, P.B., Padilla-Camberos, E., Díaz, É.F.,
684 Flores-Fernández, J.M., Ávila-Gónzalez, D., Diaz-Martinez, N.E., 2019.
685 Implications of human induced pluripotent stem cells in metabolic disorders:
686 from drug discovery toward precision medicine. Drug. Discov. Today. 24, 334-
687 341. https://doi.org/10.1016/j.drudis.2018.10.001.
688 Danoy, M., Lereau Bernier, M., Kimura, K., Poulain, S., Kato, S., Mori, D., Kido, T.,
689 Plessy, C., Kusuhara, H., Miyajima, A., Sakai, Y., Leclerc, E., 2019. Optimized
690 protocol for the hepatic differentiation of induced pluripotent stem cells in a
691 fluidic microenvironment. Biotechnol. Bioeng. 116, 1762-1776.
692 https://doi.org/10.1002/bit.26970.
693 DeFronzo, R.A., Ferrannini, E., Groop, L., Henry, R.R., Herman, W.H., Holst, J.J., Hu,
694 F.B., Kahn, C.R., Raz, I., Shulman, G.I., Simonson, D.C., Testa, M.A., Weiss,
695 R., 2015. Type 2 diabetes mellitus. Nat. Rev. Dis. Primers. 1, 15019.
696 https://doi.org/10.1038/nrdp.2015.19.
697 Emre, N., Vidal, J.G., Elia, J., O'Connor, E.D., Paramban, R.I., Hefferan, M.P.,
698 Navarro, R., Goldberg, D.S., Varki, N.M., Marsala, M., Carson, C.T., 2010. The
699 ROCK inhibitor Y-27632 improves recovery of human embryonic stem cells
700 after fluorescence-activated cell sorting with multiple cell surface markers. PLoS
701 One. 5, e12148. https://doi.org/10.1371/journal.pone.0012148.
702 Esch, E.W., Bahinski, A., Huh, D., 2015. Organs-on-chips at the frontiers of drug

703 discovery. Nat. Rev. Drug. Discov. 14, 248-260. https://doi.org/10.1038/nrd4539.
704 Essaouiba, A., Okitsu, T., Jellali, R., Shinohara, M., Danoy, M., Tauran, Y., Legallais,
705 C., Sakai, Y., Leclerc, E., 2020. Microwell-based pancreas-on-chip model
706 enhances genes expression and functionality of rat islets of Langerhans. Mol.
707 Cell Endocrinol. 514, 110892. https://doi.org/10.1016/j.mce.2020.110892.
708 Essaouiba, A., Okitsu, T., Kinoshita, R., Jellali, R., Shinohara, M., Danoy, M.,
709 Legallais, C., Sakai, Y., Leclerc, E., 2020. Development of a pancreas-liver
710 organ-on-chip coculture model for organ-to-organ interaction studies. Biochem.
711 Eng. J. https://doi.org/10.1016/j.bej.2020.107783.
712 Galderisi, A., Schlissel, E., Cengiz, E., 2017. Keeping up with the diabetes
713 technology: 2016 endocrine society guidelines of insulin pump therapy and
714 continuous glucose monitor management of diabetes. Curr. Diab. Rep. 17, 111.
715 https://doi.org/10.1007/s11892-017-0944-6.
716 Hauge-Evans, A.C., King, A.J., Carmignac, D., Richardson, C.C., Robinson, I.C.,
717 Low, M.J., Christie, M.R., Persaud, S.J., Jones, P.M., 2009. Somatostatin
718 secreted by islet delta-cells fulfills multiple roles as a paracrine regulator of islet
719 function. Diabetes. 58, 403-411. https://doi.org/10.2337/db08-0792.
720 Heimberg, H., De Vos, A., Pipeleers, D., Thorens, B., Schuit, F., 1995. Differences in
721 glucose transporter gene expression between rat pancreatic alpha- and beta-
722 cells are correlated to differences in glucose transport but not in glucose
723 utilization. J. Biol. Chem. 270, 8971-8975.
724 https://doi.org/10.1074/jbc.270.15.8971.
725 Hirano, K., Konagaya, S., Turner, A., Noda, Y., Kitamura, S., Kotera, H., Iwata, H.,
726 2017. Closed-channel culture system for efficient and reproducible
727 differentiation of human pluripotent stem cells into islet cells. Biochem. Biophys.
728 Res. Commun. 487, 344e350. https://doi.org/10.1016/j.bbrc.2017.04.062.
729 Hohwieler, M., Müller, M., Frappart, P.O., Heller, S., 2019. Pancreatic progenitors
730 and organoids as a prerequisite to model pancreatic diseases and cancer. Stem
731 Cells Int. 2019, 9301382. https://doi.org/10.1155/2019/9301382.
732 Hosoya, M., 2012. Preparation of pancreatic β-cells from human iPS cells with small
733 molecules. Islets. 4, 249-252. https://doi.org/10.4161/isl.20856.
734 International Diabetes Federation, IDF Diabetes Atlas, 9th edn. 2019.
735 https://www.diabetesatlas.org/en/ (accessed may 2020).

736 Jellali, R., Bricks, T., Jacques, S., Fleury, M.J., Paullier, P., Merlier, F., Leclerc, E.,
737 2016. Long-term human primary hepatocyte cultures in a microfluidic liver biochip
738 show maintenance of mRNA levels and higher drug metabolism compared with
739 Petri cultures. Biopharm. drug dispos. 37, 264-275.
740 https://doi.org/10.1002/bdd.2010.
741 Jellali, R., Essaouiba, A., Leclerc, E., Legallais, C., 2020. Membrane bioreactors for
742 bio-artificial pancreas, in: Basile, A., Annesini, M.C., Piemonte, V., Charcosset,
743 C., (Eds.), Current Trends and Future Developments on (Bio-) Membranes,
744 Elsevier, pp. 77-108. https://doi.org/10.1016/B978-0-12-814225-7.00004-8.
745 Jellali, R., Fleury, M.J., Paullier, P., Leclerc, E., 2016. Liver and kidney cells cultures
746 in a new perfluoropolyether biochip. Sens. Actuator B-Chem. 229, 396-407.
747 https://doi.org/10.1016/j.snb.2016.01.141.
748 Jun, Y., Lee, J., Choi, S., Yang, J.H., Sander, M., Chung, S., Lee, S.H., 2019. In vivo-
749 mimicking microfluidic perfusion culture of pancreatic islet spheroids. Sci Adv. 5,
750 eaax4520. https://doi.org/10.1126/sciadv.aax4520.
751 Kaddis, J.S., Olack, B.J., Sowinski, J., Cravens, J., Contreras, J.L., Niland, J.C.,
752 2009. Human pancreatic islets and diabetes research. JAMA. 2009, 301, 1580–
753 1587. https://doi.org/10.1001/jama.2009.482.
754 Kahraman, S., Okawa, E.R., Kulkarni, R.N., 2016. Is transforming stem cells to
755 pancreatic beta cells still the holy grail for type 2 diabetes? Curr. Diab. Rep. 16,
756 70. https://doi.org/10.1007/s11892-016-0764-0.
757 King, A., Bowe, J., 2016. Animal models for diabetes: Understanding the
758 pathogenesis and finding new treatments. Biochem. Pharmacol. 99, 1-10.
759 https://doi.org/10.1016/j.bcp.2015.08.108.
760 Leclerc, E., Hamon, J., Claude, I., Jellali, R., Naudot, M., Bois, F., 2015. Investigation
761 of acetaminophen toxicity in HepG2/C3a microscale cultures using a system
762 biology model of glutathione depletion. Cell Biol. Toxicol. 31, 173-185.
763 https://doi.org/10.1007/s10565-015-9302-0.
764 Lee, S.H., Hong, S., Song, J., Cho, B., Han, E.J., Kondapavulur, S., Kim, D., Lee,
765 L.P., 2018. Microphysiological analysis platform of pancreatic islet β-cell
766 spheroids. Adv. Healthc. Mater. 7, 1701111.
767 https://doi.org/10.1002/adhm.201701111.

Li, X., Brooks, J.C., Hu, J., Ford, K.I., Easley, C.J., 2017. 3D-templated, fully automated microfluidic input/output multiplexer for endocrine tissue culture and secretion sampling. Lab Chip. 17, 341-349. https://doi.org/10.1039/c6lc01201a.

Li, Z., Sun, H., Zhang, J., Zhang, H., Meng, F., Cui, Z., 2013. Development of in vitro 3D TissueFlex® islet model for diabetic drug efficacy testing. PLoS One. 8, e72612. https://doi.org/10.1371/journal.pone.0072612.

MacDonald, M.J., Longacre, M.J., Stoker, S.W., Kendrick, M., Thonpho, A., Brown, L.J., Hasan, N.M., Jitrapakdee, S., Fukao, T., Hanson, M.S., Fernandez, L.A., Odorico, J., 2011. Differences between human and rodent pancreatic islets: low pyruvate carboxylase, atp citrate lyase, and pyruvate carboxylation and high glucose-stimulated acetoacetate in human pancreatic islets. J. Biol. Chem. 286, 18383-18396. https://doi.org/10.1074/jbc.M111.241182.

Matschinsky, F.M., Wilson, D.F., 2019. The central role of glucokinase in glucose homeostasis: A perspective 50 Years after demonstrating the presence of the enzyme in islets of Langerhans. Front. Physiol. 10, 148. https://doi.org/10.3389/fphys.2019.00148.

Matsuoka, T.A., Kawashima, S., Miyatsuka, T., Sasaki, S., Shimo, N., Katakami, N., Kawamori, D., Takebe, S., Herrera, P.L., Kaneto, H., Stein, R., Shimomura, I., 2017. Mafa enables Pdx1 to effectively convert pancreatic islet progenitors and committed islet α-cells into β-cells in vivo. Diabetes. 66, 1293-1300. https://doi.org/10.2337/db16-0887.

Merlier, F., Jellali, R., Leclerc, E., 2017. Online hepatic rat metabolism by coupling liver biochip and mass spectrometry. Analyst. 142, 3747-3757. https://doi.org/10.1039/C7AN00973A.

Millman, J.R., Pagliuca, F.W., 2017. Autologous pluripotent stem cell–derived b-like cells for diabetes cellular therapy. Diabetes. 66, 11111120. https://doi.org/10.2337/db16-1406.

Millman, J.R., Xie, C., Van Dervort, A., Gürtler, M., Pagliuca, F.W., Melton, D.A., 2016. Generation of stem cell-derived b-cells from patients with type 1 diabetes. Nat. Commun. 7, 11463. https://doi.org/10.1038/ncomms11463.

Mohammed, J.S., Wang, Y., Harvat, T.A., Oberholzer, J., Eddington, D.T., 2009. Microfluidic device for multimodal characterization of pancreatic islets. Lab Chip. 9, 97-106. https://doi.org/10.1039/B809590F.

Pagliuca, F.W., Millman, J.R., Gurtler, M., Segel, M., Van Dervort, A., Hyoje, R.J., Peterson, Q.P., Greiner, D., Melton, D.A., 2014. Generation of functional human pancreatic β cells in vitro. Cell. 159, 428-439. https://doi.org/10.1016/j.cell.2014.09.040.

Pellegrini, S., Manenti, F., Chimienti, R., Nano, R., Ottoboni, L., Ruffini, F., Martino, G., Ravassard, P., Piemonti, L., Valeria Sordi, V., 2018. Differentiation of sendai virus-reprogrammed iPSC into β cells, compared with human pancreatic islets and immortalized β cell line. Cell Transplant. 27, 1548-1560. https://doi.org/10.1177/0963689718798564.

Prot, J.M., Aninat, C., Griscom, L., Razan, F., Brochot, C., Guguen Guillouzo, C., Legallais, C., Corlu, A., Leclerc, E., 2011. Improvement of HepG2/C3a cell functions in a microfluidic biochip. Biotechnol. Bioeng. 108, 1704-1715. https://doi.org/10.1002/bit.23104.

Puri, S., Folias, A.E., Hebrok, M., 2015. Plasticity and dedifferentiation within the pancreas: development, homeostasis, and disease. Cell Stem Cell. 16, 18-31. https://doi.org/10.1016/j.stem.2014.11.001.

Rogal, J., Zbinden, A., Schenke-Layland, K., Loskill, P., 2019. Stem-cell based organ-on-a chip models for diabetes research. Adv. Drug Deliv. Rev. 140, 101-128. https://doi.org/10.1016/j.addr.2018.10.010.

Sankar, K.S., Green, B.J., Crocker, A.R., Verity, J.E., Altamentova, S.M., Rocheleau, J.V., 2011. Culturing pancreatic islets in microfluidic flow enhances morphology of the associated endothelial cells. PloS One. 6, e24904. https://doi.org/10.1371/journal.pone.0024904.

Schaffer, A.E., Freude, K.K., Nelson, S.B., Sander, M., 2010. Ptf1a and Nkx6 transcription factors function as antagonistic lineage determinants in multipotent pancreatic progenitors. Dev. Cell. 18, 1022-1029. https://doi.org/10.1016/j.devcel.2010.05.015.

Scharfmann, R., Staels, W., Albagli, O., 2019. The supply chain of human pancreatic β cell lines. J. Clin. Invest. 129, 3511-3520. https://doi.org/10.1172/JCI129484.

Schulze, T., Mattern, K., Früh, E., Hecht, L., Rustenbeck, I., Dietzel, A., 2017. A 3D microfluidic perfusion system made from glass for multiparametric analysis of stimulus-secretion coupling in pancreatic islets. Biomed. Microdevices. 19, 47. https://doi.org/10.1007/s10544-017-0186-z.

834 Shinohara, M., Kimura, H., Montagne, K., Komori, K., Fujii, T., Sakai, Y., 2014.
835 Combination of microwell structures and direct oxygenation enables efficient and
836 size-regulated aggregate formation of an insulin-secreting pancreatic beta-cell
837 line. Biotechnol. Prog. 30, 178-187. https://doi.org/10.1002/btpr.1837.
838 Shinohara, M., Komori, K., Fujii, T., Sakai, Y., 2017. Enhanced self-organization of
839 size controlled hepatocytes aggregates on oxygen permeable honeycomb
840 microwell sheets. Biomed. Phys. Eng. Express. 3, 045016.
841 https://doi.org/10.1088/2057-1976/aa7c3d.
842 Southard, S.M., Kotipatruni, R.P., Rust, W.L., 2018. Generation and selection of
843 pluripotent stem cells for robust differentiation to insulin-secreting cells capable of
844 reversing diabetes in rodents. PloS One. 13, e0203126.
845 https://doi.org/10.1371/journal.pone.0203126.
846 Spence, J.R., Wells, J.M., 2007. Translational embryology: using embryonic
847 principles to generate pancreatic endocrine cells from embryonic stem cells. Dev.
848 Dyn. 236, 3218-3227. https://doi.org/10.1002/dvdy.21366.
849 Takahashi, K., Tanabe, K., Ohnuki, M., Narita, M., Ichisaka, T., Tomoda, K.,
850 Yamanaka, S., 2007. Induction of pluripotent stem cells from adult human
851 fibroblasts by defined factors. Cell. 131, 861-872.
852 https://doi.org/10.1016/j.cell.2007.11.019.
853 Tao, T., Wang, Y., Chen, W., Li, Z., Su, W., Guo, Y., Deng, P., Qin, J., 2019.
854 Engineering human islet organoids from iPSCs using an organ-on-chip platform.
855 Lab Chip. 19, 948-958. https://doi.org/10.1039/C8LC01298A.
856 Watanabe, K., Ueno, M., Kamiya, D., Nishiyama, A., Matsumura, M., Wataya, T.,
857 Takahashi, J.B., Nishikawa, S., Muguruma, K., Sasai, Y., 2007. A ROCK inhibitor
858 permits survival of dissociated human embryonic stem cells. Nat. Biotechnol. 25,
859 681-686. https://doi.org/10.1038/nbt1310.
860 Yabe, S., Fukuda, S., Takeda, F., Nashiro, K., Shimoda, M., Okochi, H., 2017.
861 Efficient generation of functional pancreatic β-cells from human induced
862 pluripotent stem cells. J. Diabetes. 9, 168-179. https://doi.org/10.1111/1753-
863 0407.12400.
864 Young, E., Beebe, D., 2010. Fundamentals of microfluidic cell culture in controlled
865 microenvironments. Chem. Soc. Rev. 39, 1036-1048.
866 https://doi.org/10.1039/b909900j.

Yu, H., Alexander, C., Beebe, D., 2007. Understanding microchannel culture: parameters involved in soluble factor signaling. Lab Chip. 7, 726-30. https://doi.org/10.1039/b618793e.

Zbinden, A., Marzi, J., Schlünder, K., Probst, C., Urbanczyk, M., Black, S., Brauchle, E.M., Layland, S.L., Kraushaar, U., Duffy, G., Schenke-Layland, K., Loskill, P., 2020. Non-invasive marker-independent high content analysis of a microphysiological human pancreas-on-a-chip model. Matrix Biol. 85-86, 205-220. https://doi.org/10.1016/j.matbio.2019.06.008.

Zhu, S., Russ, H., Wang, X., Zhang, M., Ma, T., Xu, T., Tang, S., Hebrok, M., Ding, S., 2016. Human pancreatic beta-like cells converted from fibroblasts. Nat. Commun. 7, 10080. https://doi.org/10.1038/ncomms10080.

Figures Captions

Fig.1. (A) Schematic of differentiation process from hiPSC to beta cells; (B) experimental procedures used for stage 2 of β-cells maturation.

Fig.2. Design and structure of (A) honeycomb and (B) biochips used for hiPSC derived β-cells cultures.

Fig.3. hiPSC derived β-cells cultures in static Petri (monolayer). (A-C) morphologies after 5 h, 12 and 16 days, respectively; (D-G) immunostainings of β-cells at the end of the experiment: DAPI, MAFA, PDX1 and insulin, respectively; (H) ratio of mRNA levels (iPSC derived β-cells/iPSC) of selected genes after 24h and 16 days of culture, *$P < 0.05$ mRNA level significantly different when compared to iPSCs; (I) daily C-peptide secretion.

Fig.4. Morphology of hiPSC derived β-cells cultivated in honeycomb wells and microfluidic biochips. (A) 2D (monolayer) dynamic culture in biochip; (B) 3D (spheroids) static culture in honeycomb wells seeded at low- and high-density of cells; (C) 3D (spheroids) dynamic culture in biochip after 14 days of culture (4 days in static honeycomb and 10 days in biochip).

Fig.5. Immunostainings (end of the experiments) of hiPSC derived β-cells spheroids cultivated in honeycomb wells and biochips (A) DAPI, insulin, glucagon and merge; (B) DAPI, PAFA, PDX1 and merge.

Fig.6. hiPSC derived β-cells spheroids cultivated at high- and low-density in static honeycomb wells. (A) daily c-peptide secretion between day 9 and day 14; (B) daily insulin secretion at day 14 (*$P < 0.05$); (C) ratio of insulin secretion (high/low, GSIS index) after high/low glucose stimulations (*$P < 0.05$, GSIS:

glucose-stimulated insulin secretion); (D) ratio (GLP1/control) of insulin secretion after GLP1 treatment.

Fig.7. Ratio of mRNA levels of selected genes at the end of culture. black bars: β-cells spheroids cultivated at high-density in static honeycomb wells versus β-cells cultures in static Petri (2D monolayer) and gray bars: β-cells spheroids cultivated in dynamic biochip versus β-cells cultures in static Petri (2D monolayer). *P < 0.05, mRNA level significantly different when compared to static Petri (2D monolayer.

Fig.8. hiPSC derived β-cells spheroids cultivated in honeycomb wells (high-density) and biochips. (A) daily c-peptide secretion between day 9 and day 14 (*P < 0.05); (B) daily insulin secretion at day 14 (*P < 0.05); (C) ratio of insulin secretion (high/low, GSIS index) after high/low glucose stimulations (GSIS: glucose-stimulated insulin secretion); (D) ratio (GLP1/control) of insulin secretion after GLP1 treatment.

Figure 1

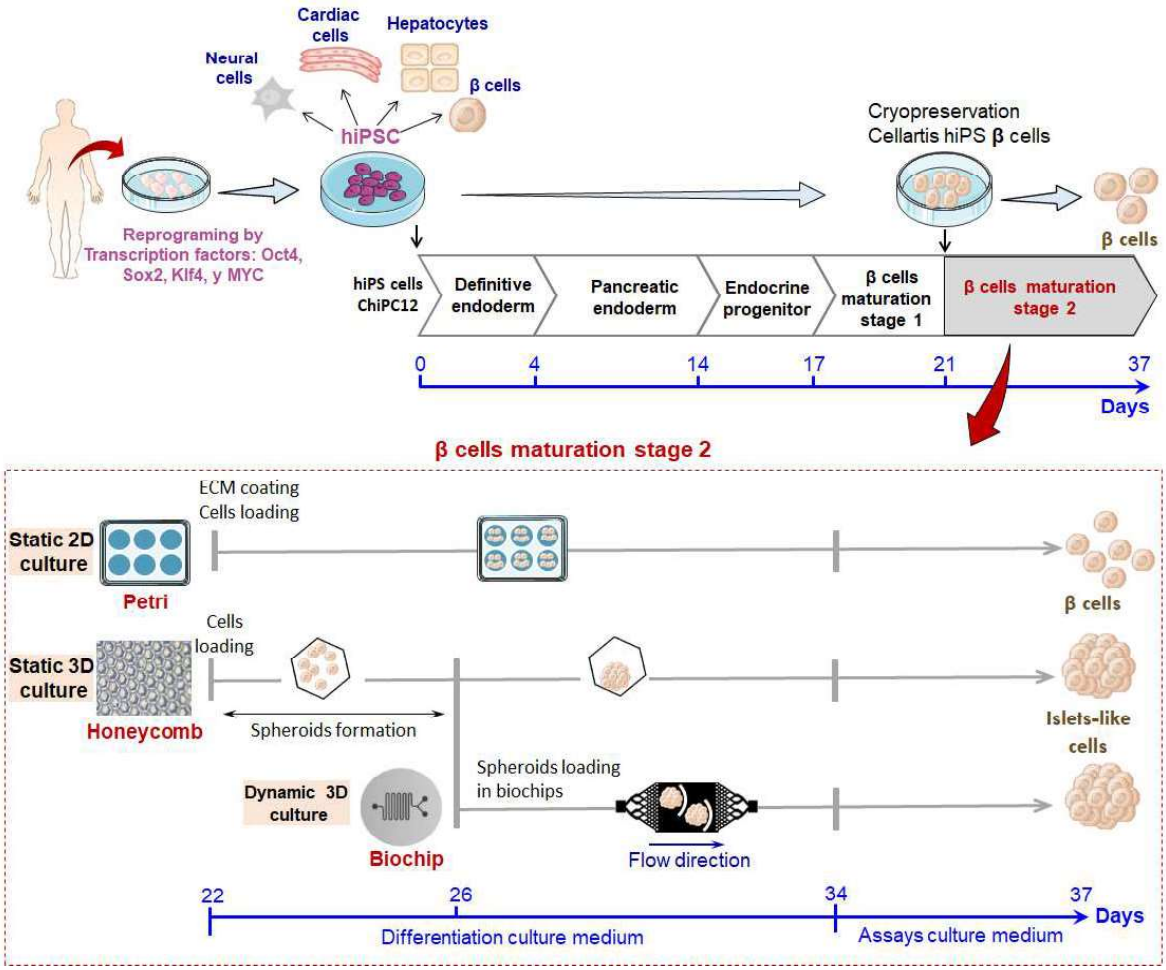

Fig.1

Figure 2

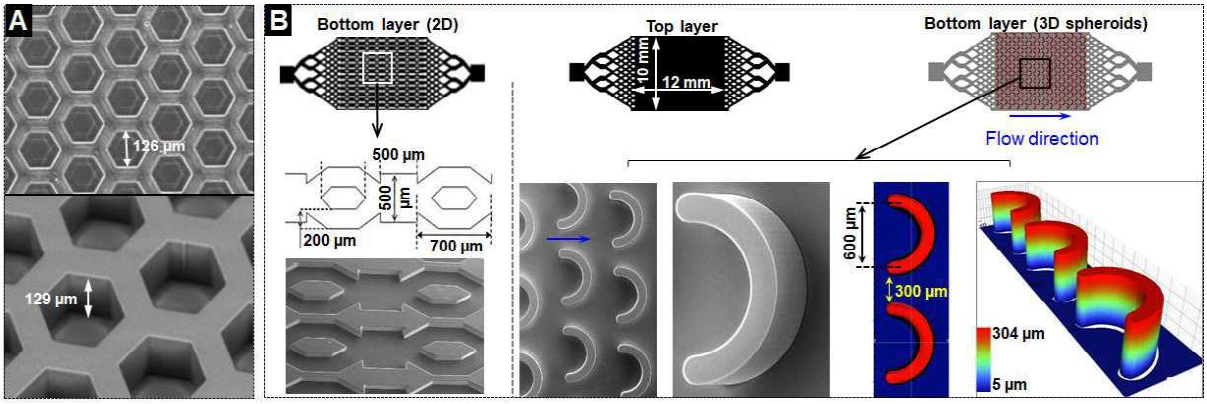

Fig.2

Figure 3

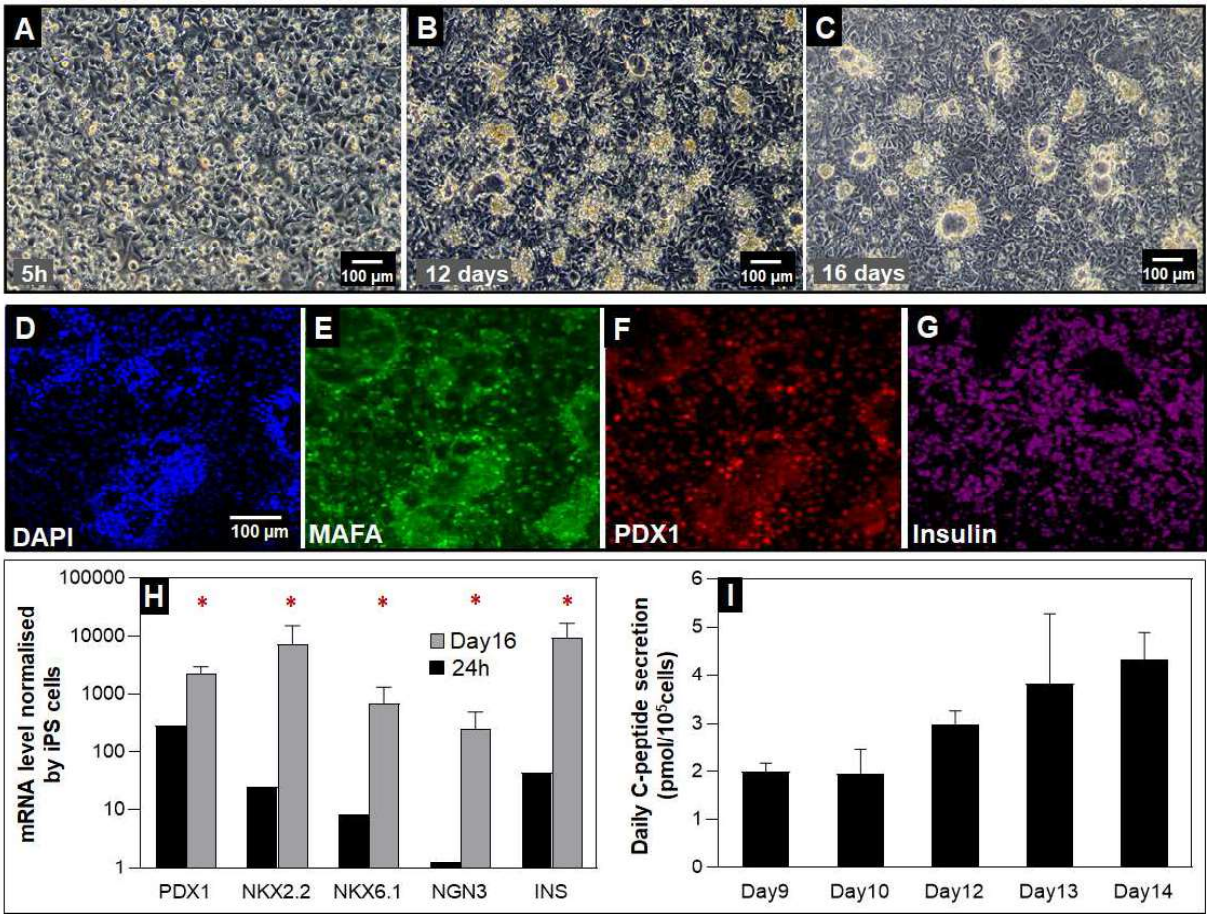

Fig.3

Figure 4

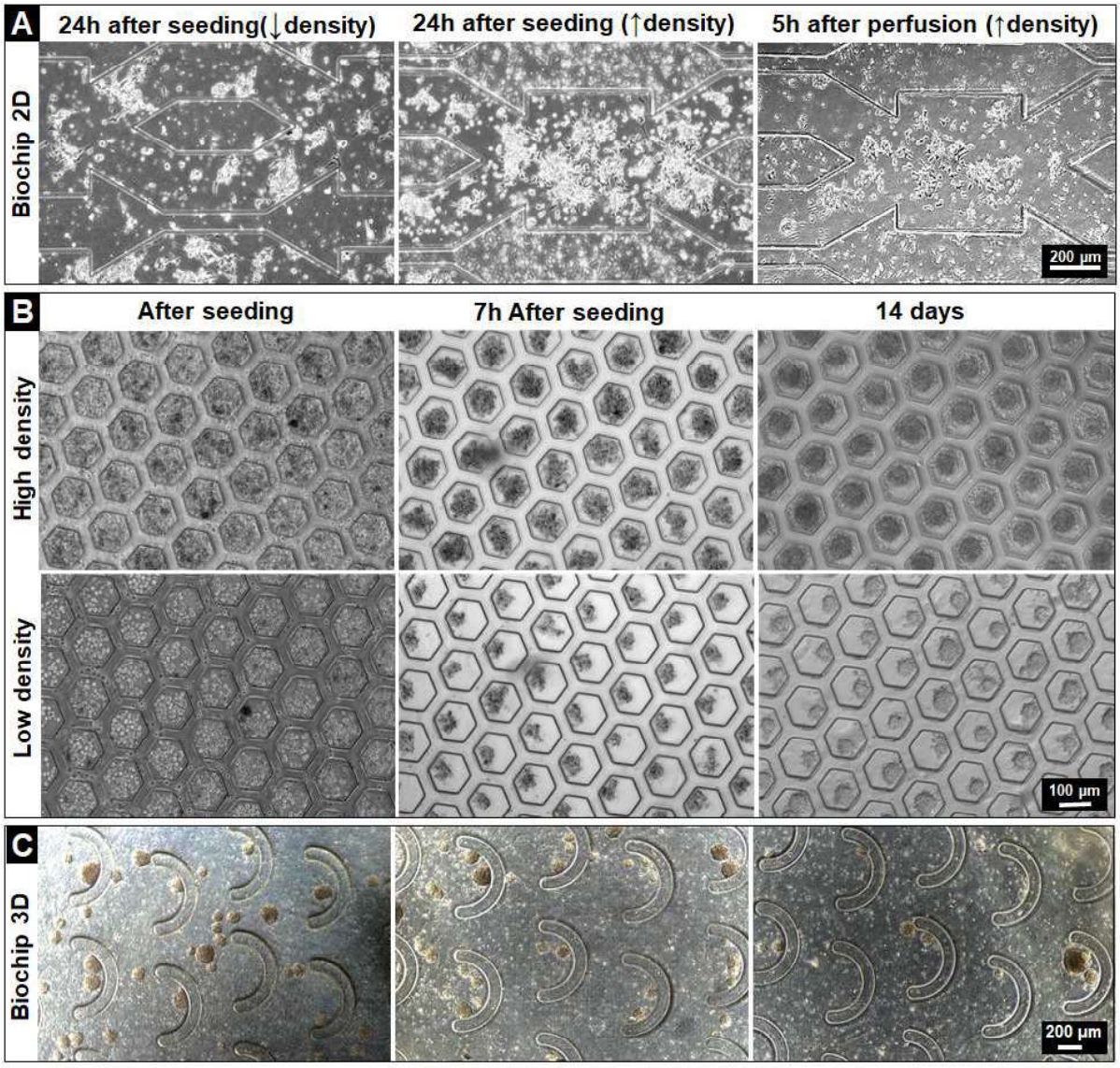

Fig.4

Figure 5

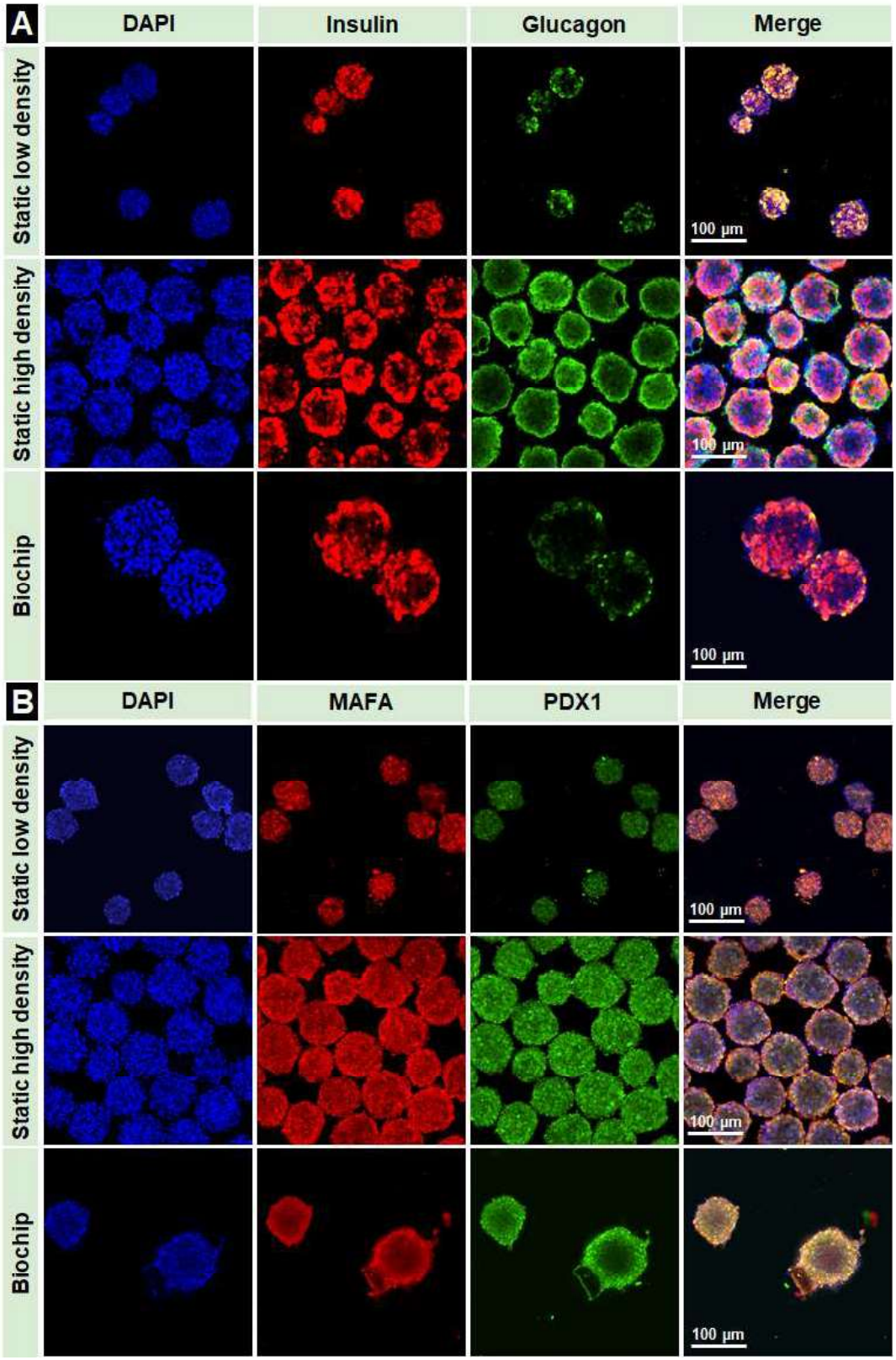

Fig.5

Figure 6

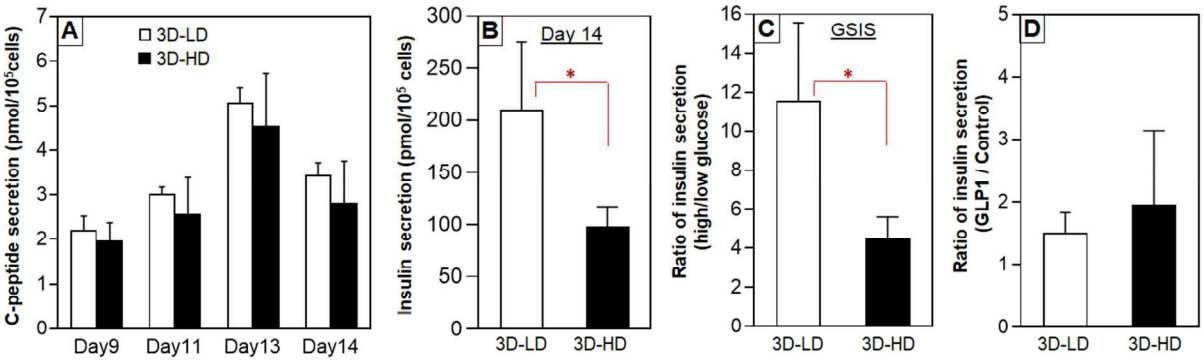

Fig.6

Figure 7

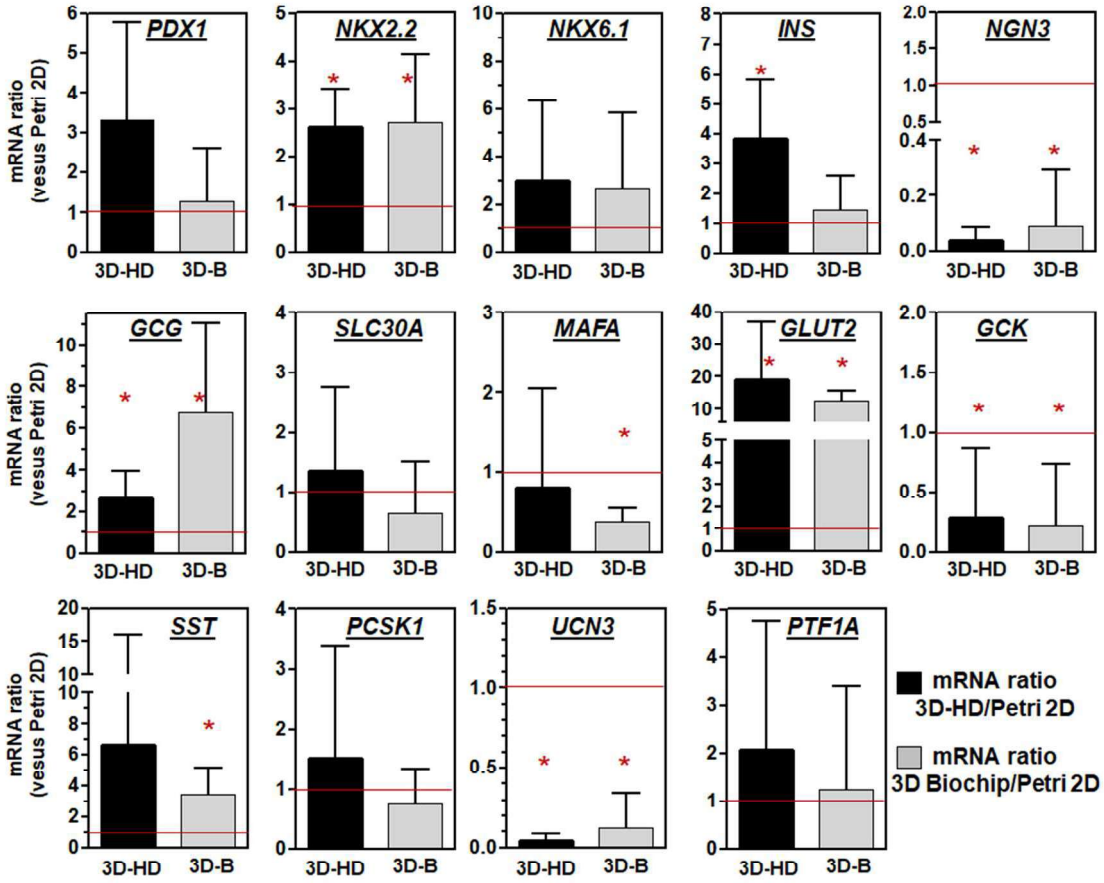

Fig.7

Figure 8

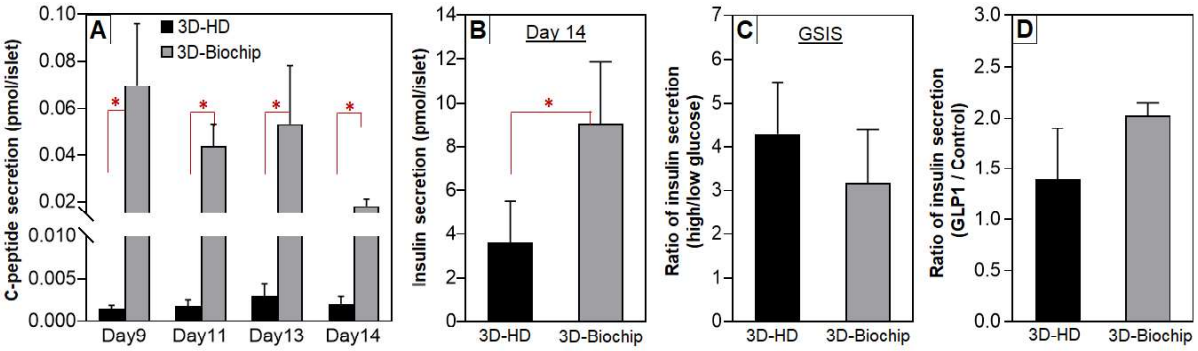

Fig.8